Int J Appl Earth Obs Geoinformation 64 (2018) 132–144

Contents lists available at ScienceDirect

Int J Appl Earth Obs Geoinformation

journal homepage: www.elsevier.com/locate/jag

MODIS-derived EVI, NDVI and WDRVI time series to estimate phenological metrics in French deciduous forests

S. Testa[a,*], K. Soudani[b], L. Boschetti[c], E. Borgogno Mondino[a]

[a] Department of Agricultural, Forest and Food Sciences, University of Turin, Grugliasco (TO), Italy
[b] Univ. Paris-Sud, Laboratoire Ecologie Systématique et Evolution, UMR8079, F-91405. CNRS, Orsay, France
[c] Department of Natural Resources and Society, University of Idaho, Moscow, ID, USA

ARTICLE INFO

Keywords:
Forest phenology
MODIS time series
EVI
WDRVI
NDVI

ABSTRACT

Monitoring forest phenology allows us to study the effects of climate change on vegetated land surfaces. Daily and composite time series (TS) of several vegetation indices (VIs) from MODerate resolution Imaging Spectroradiometer (MODIS) data have been widely used in scientific works for phenological studies since the beginning of the MODIS mission. The objective of this work was to use MODIS data to find the best VI/TS combination to estimate start-of-season (SOS) and end-of-season (EOS) dates across 50 temperate deciduous forests. Our research used as inputs 2001–2012 daily reflectance from MOD09GQ/MOD09GA products and 16-day composite VIs from the MOD13Q1 dataset. The 50 pixels centered on the 50 forest plots were extracted from the above-mentioned MODIS imagery; we then generated 5 different types of TS (1 daily from MOD09 and 4 composite from MOD13Q1) and used all of them to implement 6 VIs, obtaining 30 VI/TS combinations. SOS and EOS estimates were determined for each pixel/year and each VI/TS combination. SOS/EOS estimations were then validated against ground phenological observations. Results showed that, in our test areas, composite TS, if actual acquisition date is considered, performed mostly better than daily TS. EVI, $WDRVI_{0.20}$ and NDVI were more suitable to SOS estimation, while $WDRVI_{0.05}$ and EVI were more convenient in estimating early and advanced EOS, respectively.

1. Introduction

The concept of phenology was initially introduced by Morren (1849) as “the science having the goal to understand the manifestations of life governed by time” (Demarée and Rutishauser, 2009). Phenology is currently defined by the United States International Biological Program Committee as the study of (a) the timing of recurring biological events; (b) the causes of their timing with regard to biotic and abiotic forces; and, (c) the interrelation among phases of the same or different species (Lieth, 1974). Surveying forest phenology requires the observation of the timing of events such as bud burst, and leaves emerging, developing and falling (Liang and Schwartz, 2009; Nordli et al., 2008; Richardson et al., 2013; Thomas et al., 2010).

Adopting the terminology commonly used in previous studies, phenological stages are defined as the developmental stages of an organism's life cycle (Ruml and Vulić, 2005); the corresponding measurement is the date of occurrence, i.e. the date in which the phenological stage is first observed. Phenological phases are defined as the time interval between the date of occurrence of two consecutive phenological stages (Ruml and Vulić, 2005).

Accurate long-term monitoring of plant phenology at global and continental scales allows the evaluation of the interactions and feedback between climate and vegetation (Bradley et al., 1999; Fabian and Menzel, 1998; Koch et al., 2008; Richardson et al., 2013; Schwartz, 1998). Vegetation phenology is responsive to environmental and climatic dynamics (Crucifix et al., 2005; Penuelas and Filella, 2001), but also influences them (Penuelas et al., 2009; Richardson et al., 2013), with repercussions on water and biogeochemical cycles (Cowie, 2007; Gu et al., 2003; Noormets, 2009). At the single-plant or stand scale, vegetation phenology is affected by individuals' traits (genes, age), soil (temperature, nutrients, flora, fauna, wetness), pests, diseases, intra- and extra-specific competition, micro-climate, water availability, pollinators and other factors (Defila, 1992; Elzinga et al., 2007; Fenner, 1998). At the macro-scale, temperature (Brooke et al., 1996), photoperiod (Vitasse and Basler, 2013) and precipitation (Lieberman and Milton, 1984) are the main phenological drivers (Fenner, 1998; Keatley and Fletcher, 2003; Sarvas, 1972, 1974), that are affected in turn by the biome and its vegetation.

Numerous phenological studies found earlier onset of plant growth and longer vegetative season at mid and high latitudes in the northern

* Corresponding author.
E-mail address: stefano.testa@hotmail.com (S. Testa).

http://dx.doi.org/10.1016/j.jag.2017.08.006
Received 28 October 2015; Received in revised form 27 July 2017; Accepted 10 August 2017
Available online 18 September 2017
0303-2434/

hemisphere (European Environment Agency, 2004, 2012; Koch et al., 2008; Menzel and Fabian, 1999; Nordli et al., 2008; Parmesan and Galbraith, 2004; Rosenzweig et al., 2007; Schaber and Badeck, 2005; Henebry, 2013).

Other phenological studies demonstrated that phenological stages in temperate forests begin and totally develop in 7–33 days (Aubinet et al., 2002; Bequet et al., 2011; Breda et al., 1995; Brügger et al., 2003; Gond et al., 1999; Granier et al., 2000; Soudani et al., 2012). A review of phenological trends is available in Richardson et al. (2013).

Remote sensing is a key instrument in global monitoring (Reed et al., 2003) in that a number of satellite missions guarantee repeated, periodic observations of the Earth's entire surface from a very unique point of view. In fact, satellites provide near-global observations of the climate system, and they are playing a major role in global climate observing (World Meteorological Organization, 2006). Ongoing climate change sets an important objective for the remote sensing phenology-oriented scientific community: to estimate the timing of phenological stages accurately and precisely enough to remedy the lack of ground surveys. Field measurements will always be essential to validate estimates based on space data (Beaubien and Hall-Beyer 2003), despite the issue of the different reference scale (a "point" in ground surveys, an area in satellite acquisitions) (Morisette et al., 2009).

Land surface phenology (LSP) monitoring from satellite data relies on the availability of large series of consistent, spatially coincident observations, and it is mostly conducted through time series (TS) analysis (Ahl et al., 2006; Bradley et al., 2007; Busetto et al., 2010; Colombo et al., 2011; Colombo et al., 2009; de Beurs and Henebry, 2004; Gutman et al., 1995; Jönsson and Eklundh, 2002; Jönsson and Eklundh, 2003). Typically, satellite data are preprocessed by applying a fitting/smoothing algorithm, and then a set of criteria is applied to estimate the timing of the phenological stages. When considering temporal trends in phenological metrics, attention should be paid to their reliable detection (de Beurs and Henebry, 2005).

Among the available RS data, NASA's sensors MODerate resolution Imaging Spectroradiometer (MODIS) onboard the Terra and Aqua satellites have been widely used in a variety of studies (Ahl et al., 2006; Busetto et al., 2010; Colombo et al., 2011; Colombo et al., 2009; Hmimina et al., 2013; Eklundh et al., 2009; Sesnie et al., 2012; Song et al., 2013; Soudani et al., 2008; Zhang et al., 2003). Thanks to the two twin MODIS instruments, MODIS data are acquired globally twice per day per instrument at the spatial resolutions of 250 m, 500 m and 1 km at nadir, depending on the spectral band. MODIS imagery is distributed at various pre-processing levels and, with respect to the temporal resolution, data are released as both daily and composites products, the latter generated at different compositing steps (8-day, 16-day, monthly). Composite data have some advantages respective to daily data because the compositing process strongly reduces the effect of clouds, snow and noise (Holben, 1986; Solano et al., 2010; Wolfe et al., 1998). On the other hand, the compositing process introduces temporal and spatial discontinuities since values from adjacent pixels may have been acquired on different dates, according to quality criteria. Moreover, the temporal resolution is degraded and may not be sufficient to accurate monitoring of rapid transitions in vegetation dynamics (Ahl et al., 2006; Holben, 1986; Solano et al., 2010), especially in cases of compositing periods longer than 16 days (Zhang et al., 2009).

Various algorithms have been developed to model the behavior through time of physiological variables that can be tracked by satellite data, such as LAI (Leaf Area Index), FPAR (Fraction of Photosynthetically Active Radiation) or chlorophyll content (Rodriguez-Galiano et al., 2015). According to the available literature, in deciduous forests characterized by large seasonal changes in canopy leaf area, methods based on least-square fitting of logistic functions of time applied on time-series of satellite-derived vegetation indices led to estimations close to ground observations (Hird and McDermid, 2009; White et al., 2009; Atkinson et al., 2012). Those methods use analogy with phenology and growing degree-day models based on the assumption that vegetation phenology and growing are responsive to cumulative daily temperature, which can be represented by a logistic function of time (de Beurs and Henebry, 2010a; Ratkowsky, 1983; Richardson et al., 2006; Villegas et al., 2001; Zhang et al., 2003). A number of different logistic functions have been used to derive the phenology information (Beck et al., 2006; Fisher et al., 2006; Hmimina et al., 2013; Soudani et al., 2008; Zhang et al., 2003) with the main differences between them being the phenological metrics considered, metrics algorithm extraction and the number of fitting parameters (four to eight). The logistic function proposed by Hmimina et al. (2013) is the one we implemented in this work since it is the latest improvement of the function proposed in Soudani et al. (2008) that in turn was based on the equation proposed by Zhang et al. (2003), the latter being that used in MODIS global vegetation phenology product (MCD12Q2). Several methods have been developed to extract Start of Season (SOS) and End of Season (EOS) dates from fitted vegetation index time-series (VI TS) generated from satellite data. TIMESAT (Jönsson and Eklundh, 2002; Jönsson and Eklundh, 2003; Jönsson and Eklundh,2004) extracts SOS and EOS according to fixed, user-defined thresholds as increase from spring minimum and decrease from summer maximum (nsson and Eklundh, 2002, 2004; nsson and Eklundh, 2002, 2004). Zhang et al. (2003) and Ahl et al. (2006) used local minima and maxima of fitting functions' curvature to find onset and fullness of flushing and yellowing. Left and right inflection points derived from logistic functions were commonly used to represent SOS and EOS respectively (Beck et al., 2006; Fisher et al., 2006; Hmimina et al., 2013; Liang et al., 2011; Soudani et al., 2008). Since inflection points are in the middle of the function's amplitude (Fisher et al., 2006; Soudani et al., 2008), they are equivalent to the TIMESAT fitting based on the logistic function algorithm with both SOS and EOS thresholds set to 0.50. Fixed VI thresholds were tested and compared to other extraction methods, sometimes with results more related to ground phenology respective to the others (Studer et al., 2007), but a universally applicable VI threshold has not yet been recognized. A review is available in de Beurs and Henebry (2010b). In addition to the fact that there is no clear consensus on the most efficient extraction algorithms, there are no conclusions that emerge clearly from previous studies regarding the best performing VIs and the uncertainty of satellite-based estimates of phenological dates related to temporal resolution used in time-series composite data.

The aim of this work was to find the best combination of MODIS imagery and VI to estimate SOS and EOS. We used 2001–2012 daily reflectance and 16-day composite Normalized Difference Vegetation Index (NDVI) and Enhanced Vegetation Index (EVI) to generate TS of six vegetation indices (EVI, NDVI and four Wide Dynamic Range Vegetation Index (WDRVI)). From each VI/TS combination we extracted SOS and EOS and then compared them with eight ground phenological metrics measured in 50 plots composed by the main deciduous broad-leaf tree species belonging to the French RENECOFOR network (*Réseau National de suivi à long terme des ECOsystèmes FORestiers*).

2. Data

2.1. Study area

The study area was composed of 50 broadleaf forest plots, distributed across France (Fig. 1).

All of the 50 forest plots are covered by deciduous forest and are part of the RENECOFOR network, created in 1992 by the French National Forest Service aimed at long-term monitoring of forest ecosystems. It is the French part of a wider network that includes 34 European countries. The main tree species populating the 50 plots we considered are *Quercus robur* L. (pedunculate oak, 9 plots); *Quercus petrae* (Matt.) Liebl. (sessile oak, 19 plots); and *Fagus sylvatica* L. (beech, 20 plots). In two plots, pedunculate and sessile oaks are mixed. Ages range from 60 to 120 years; all plots have little or no slope.

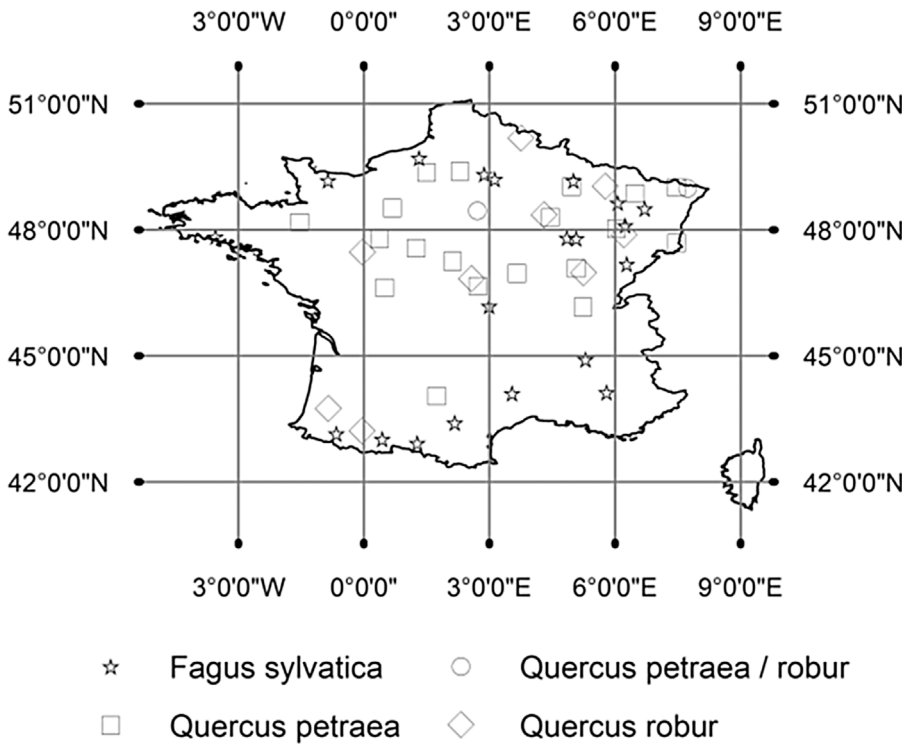

Fig. 1. Locations within France of the 50 study plots.

Climate across the plots is generally temperate, with four climatic types: a) Mediterranean, on the south coast; b) Oceanic, along the west coast; c) Continental, in the inner part of the country; and, d) Alpine, at the highest elevations (Soudani et al., 2008). Elevation of the plots range from 20 to 320 m a.s.l. (200 m on average) for oak plots and 50 to 1400 m for beech plots (560 m on average). Each plot extends over 2 ha and is covered by same-species and mature trees; 36 trees in the center of each plot are numbered, fenced and, in spring and autumn, monitored weekly. Each weekly observation is reported on the Monday of the week it refers to. Phenology of understory is monitored in the same way.

The reason we considered only deciduous vegetation is that the small yearly increase/decrease of VI values typical of evergreen canopies make logistic functions unsuitable for phenological investigations. Other methods should be used, e.g. splines (Hmimina et al., 2013).

2.2. In situ phenological observations

In this work, we compared phenological metrics (i.e. SOS, EOS) estimated from MODIS imagery with 8 types of phonological ground observations from the available stations of the RENECOFOR network (Table 1).

The 10% and 90% thresholds indicate the dates when 10% and 90% of each plot's trees have buds open (flushing phases) or yellow leaves (yellowing phases) over at least 20% of the crown (Bourjot et al., 2006). There is no official cross-walk of the RENECOFOR phenological stages to the BBCH-based phenological scale.

Table 1
Phenological stages recorded within the RENECOFOR dataset.

	Phenological Feature	Abbreviation
SOS	Main species flushing 10%	MSp F 10%
	Understory flushing 10%	Und F 10%
	Main species flushing 90%	MSp F 90%
	Understory flushing 90%	Und F 90%
EOS	Main species yellowing 10%	MSp Y 10%
	Understory yellowing 10%	Und Y 10%
	Main species yellowing 90%	MSp Y 90%
	Understory yellowing 90%	Und Y 90%

2.3. Satellite data

This work was based on 12 years (2001–2012) of both daily and composite MODIS VIs (collection 5). All the imagery was acquired from the Land Processes Distributed Active Archive Center (LP DAAC) through the Reverb-Echo portal. The 50 MODIS 250 m pixels encompassing the center of each plot were the only ones extracted from the MODIS datasets.

2.3.1. MODIS products used in the study

2.3.1.1. MOD09 GQ and MOD09GA daily surface reflectance. Daily red and near infrared (NIR) surface reflectances were acquired from the MOD09GQ (Terra) product (Surface Reflectance Daily L2G Global 250 m) at the geometric resolution of 250 m. Surface reflectances in the blue band (MODIS band 3), necessary to calculate EVI, were extracted at the 500 m resolution from the MOD09GA (Surface Reflectance Daily L2G Global 1 km and 500 m) product. In cases where multiple observations were available on the same day, we selected the first layer (LP DAAC, 2014).

Daily quality assessment (QA) flags, provided at 1 km resolution, were extracted from the MOD09GA product in order to gather information about the state of the atmosphere at the moment and in the position of the acquisition (presence of clouds, cirrus, aerosol concentration).

2.3.1.2. MOD13Q1 16-day composite vegetation indices. Composite VIs were acquired from the MOD13Q1 product (Vegetation Indices 16-day L3 Global 250 m). It provides one NDVI and EVI value every 16 days, allowing the composition of gap-free TS. The per-pixel compositing algorithm is described in the MOD13Q1 product user guide (Solano et al., 2010).

The MOD13Q1 product includes, among the other layers: a) 16-day composite EVI and NDVI; b) QA information from the layer *250 m*

16 days pixel reliability summary QA (PR); and, c) acquisition dates in the *250 m 16 days composite day of the year* layer (CDOY). The PR layer reports pixels' overall quality, while the CDOY layer contains the date each VI value was acquired. Beginning with collection 5, this layer was made available and dates are the same for both EVI and NDVI.

Within the MODIS mission, according to file names, the nominal date associated with each composite is its first day. Nevertheless, the actual acquisition date of each pixel (CDOY) usually differs from the nominal date since the acquisition may have occurred on any one of the 16 days embraced by every composite and the difference between the nominal date and the true date ranges 0–15 days. Previous research has shown that the adoption of the nominal date of composites can introduce temporal errors that potentially make a TS inadequate to correctly describe phenological patterns (Testa et al., 2014; Thayn and Price, 2008).

2.4. Vegetation indices

VIs are commonly used for extracting phenological parameters. In the present study we considered EVI, NDVI and WDRVI at four levels.

NDVI (Tucker, 1979) is the most known and used VI. Its strength is its rationing formulation, which allows the reduction of topographic effects, illumination conditions, cloud shadow and atmospheric attenuation (Huete et al., 2002). It is mainly responsive to canopy chlorophyll content. Among the limitations, NDVI is known to lose sensitivity when a canopy's Leaf Area Index is greater than 3–5 (e.g., Davi et al., 2006; Soudani et al., 2006) due to the extinction of radiation in both downward and upward directions and a reduced contribution from lower canopy layers. Within the MODIS mission, NDVI is considered the "continuity index" for the more than 20-year-long NOAA Advanced Very High Resolution Radiometer (AVHRR) mission (Huete et al., 2002). It is calculated combining NIR and red reflectances as:

$$NDVI = \frac{NIR - red}{NIR + red} \quad (1)$$

where *red* and *NIR* are MODIS band 1 and 2 surface reflectances, respectively.

EVI is the vegetation index optimized for MODIS bands (Huete et al., 1999). It has been used in phenological works, e.g. (Ahl et al., 2006; Sesnie et al., 2012; Setiawan et al., 2014), and in the MCD12Q2 MODIS product (Land Cover Dynamics Yearly L3 Global 500 m). EVI is less widely used than NDVI because it needs, in addition to red and near infrared bands, the blue one, not available for AVHRR data; the use of this vegetation index at global scale is therefore limited to MODIS data (Jiang et al., 2008).

EVI is formulated as:

$$EVI = G \cdot \frac{NIR - red}{NIR + C_1 \cdot red - C_2 \cdot blue + L} \quad (2)$$

where *blue* is the reflectance in the blue band (MODIS band 3). "*L* is the canopy background adjustment that addresses non-linear, differential NIR and red radiant transfer through a canopy, and C_1, C_2 are the coefficients of the aerosol resistance term, which uses the blue band to correct for aerosol influences in the red band" (Huete et al., 2002). The coefficients adopted to implement the MODIS EVI algorithm are: L = 1, C_1 = 6, C_2 = 7.5, and G = 2.5 (gain factor). EVI seems to be less sensitive to saturation problems over dense canopies (Hufkens et al., 2012) and reduces the influence of the background's color and atmosphere (Xiao et al., 2003).

In order to linearize the relationship between LAI and NDVI, Gitelson (2004) proposed the WDRVI. It is calculated as:

$$WDRVI = \frac{\alpha \cdot NIR - red}{\alpha \cdot NIR + red} \quad (3)$$

where α −that is lower than 1.0- is the coefficient that reduces the contribution of NIR to the VI's value. α is added to increase the contrast between red and near infrared reflected radiation by living vegetation and allows significant enhancement of the linearity and the sensitivity of WDRVI, by comparison with NDVI, especially under high biomass conditions (Gitelson, 2004). Fig. 2 shows variations in annul amplitude of WDRVI depending on α.

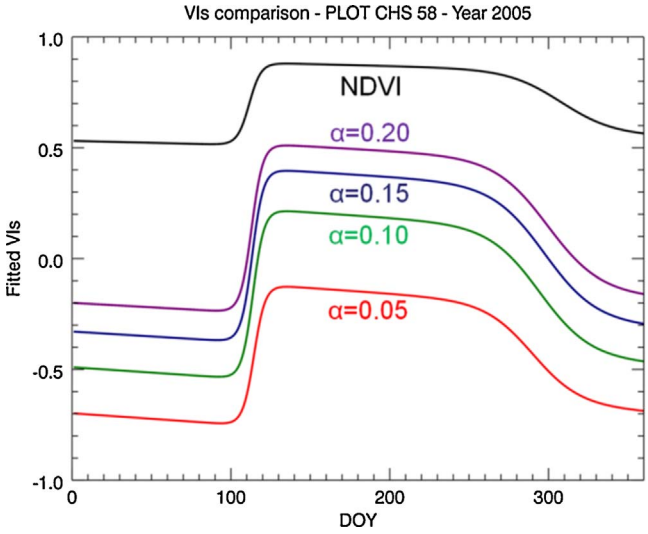

Fig. 2. Fitted TS of NDVI (black) and WDRVI as a function of the α parameter (red, green, blue, purple) of the plot CHS 58, year 2005. (For interpretation of the references to colour in this figure legend, the reader is referred to the web version of this article.)

By rearranging the terms of Eq. (3), WDRVI can be calculated as a function of NDVI (Viña and Gitelson, 2005):

$$WDRVI = \frac{(\alpha + 1) \cdot NDVI + (\alpha - 1)}{(\alpha - 1) \cdot NDVI + (\alpha + 1)} \quad (4)$$

with α = [0.05, 0.10, 0.15, 0.20]. WDRVI was originally introduced for agricultural monitoring, and it has not yet been extensively tested for forest phenology monitoring (Eklundh et al., 2009).

3. Data analysis

The following are the main processing steps we carried out: a) TS generation; b) reduction of noise in TS by removal of low quality observations (i.e. contaminated by clouds, shadows, aerosol) and filtering; c) estimation of SOS and EOS; and, d) quality analysis of SOS and EOS estimates by comparison with ground measurements of RENECOFOR plots.

3.1. Time series generation

Daily reflectances from the MOD09GQ/A products were used to compute daily 250 m EVI and NDVI TS. Calculation of daily EVI required 500 m blue band, combined with the 250 m red and NIR bands. WDRVI time series were generated from NDVI, as described in Eq. (4). Four WDRVI implementations were tested in this work, each one corresponding to a different value of the α coefficient: $WDRVI_{0.05}$, $WDRVI_{0.10}$, $WDRVI_{0.15}$, and $WDRVI_{0.20}$ where the value of α was expressed by the subscripts. Each VI TS came with a corresponding QA TS, extracted from the MOD09GA dataset.16-day composite EVI and NDVI TS were directly extracted from the correspondent MOD13Q1 layers, and the WDRVI was derived from the NDVI TS (eq. 4).

Four TS were generated from MOD13Q1 datasets (Fig. 3):

A.) Raw TS (hereafter $MOD13_{RAW}$), i.e. VIs as supplied by the MOD13 product. VI values were formally equidistant in time, but this was not accurate, since VI values could have been acquired at any point within the 16-day compositing period, making potential time

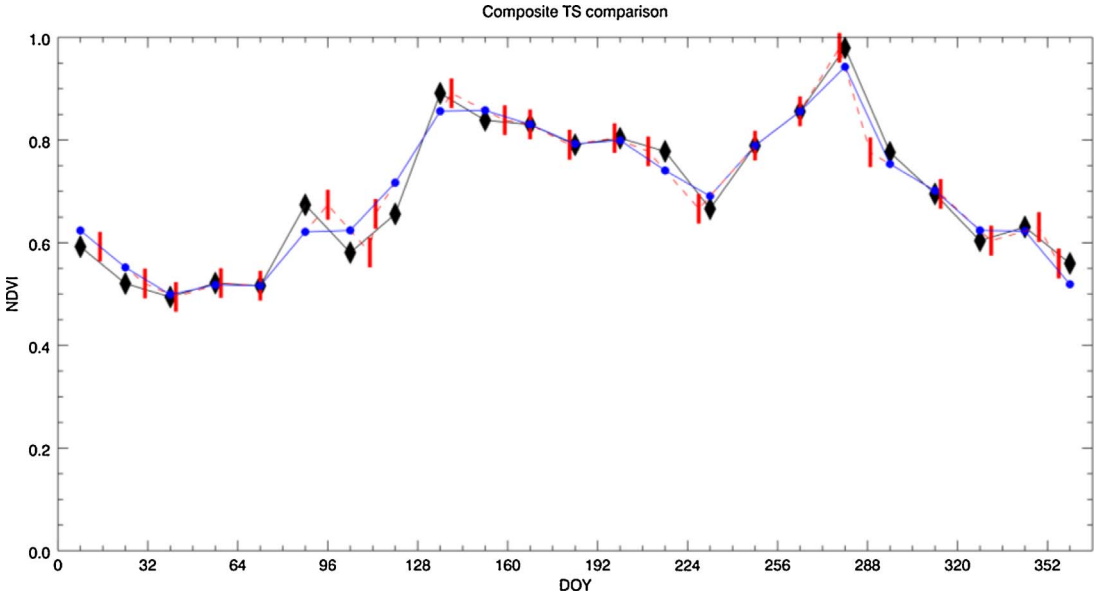

Fig. 3. NDVI TS generated from the MOD13Q1 product inherent the plot CHP10 (48°20′51" N, 4°18′17" E, elevation: 115 m a.s.l.), year 2006. Plot's main species was pedunculate oak; the understory species was hornbeam. Diamonds, solid line: $MOD13_{RAW}$ (A); vertical bar, dashed line: $MOD13_{AD}$ (B); empty circle, dotted line: $MOD13_{ALIGNED}$ (C). $MOD13_{DAILY}$ (D) is not expressly reported since it overlays MOD13AD TS.

distances between two consequent observations ranging from 1 to 31 [16 days/compositing period x 2 compositing periods – 1] days. Based on previous works (Testa et al., 2014), we considered $MOD13_{RAW}$ values nominally placed in the centre of each compositing period (the 8th day).

B.) Raw TS adjusted with regards to acquisition dates ($MOD13_{AD}$). Index values were the same as $MOD13_{RAW}$, but acquisition dates were adjusted before fitting. This resulted in a new TS not equally spaced in time.

C.) One of the assumptions of some algorithms (e.g. the Fast Fourier Transform) and software (e.g. TIMESAT) is that TS data are equidistant. According to the procedure described in Testa et al. (2014), we resampled the $MOD13_{AD}$ TS to the nominal dates (the 8th day in this work, as noted above), making it equidistant in time but with VI values linearly adjusted. TS treated according to this procedure are hereafter called $MOD13_{ALIGNED}$.

D.) The fourth way we managed composite data was aimed at creating a hybrid, pseudo-daily TS ($MOD13_{Daily}$): we performed a daily linear interpolation of the $MOD13_{AD}$ TS. The underlying idea was to create daily, gap-free TS from the less noisy composite, date-corrected $MOD13_{AD}$ TS.

3.2. TS preprocessing

Time series were preprocessed by removing observations contaminated by clouds, shadows and snow. Only pixels whose QA flags reported no contamination were considered.

Then, a moving median filter was run on daily TS to reduce noise (Hmimina et al., 2013; Soudani et al., 2008). Given a 5-day moving window, its median was calculated at each step and VI values outside the *median ± 20%* range were discarded, as proposed by Soudani et al. (2008). Fig. 4 indicates the effect of the median filter on daily NDVIs for the oak plot CHP10, year 2006.

3.3. Time series fitting and estimation of SOS and EOS

We modelled VI TS performing iterative Least Square fitting of the asymmetric double logistic function proposed by (Hmimina et al., 2013):

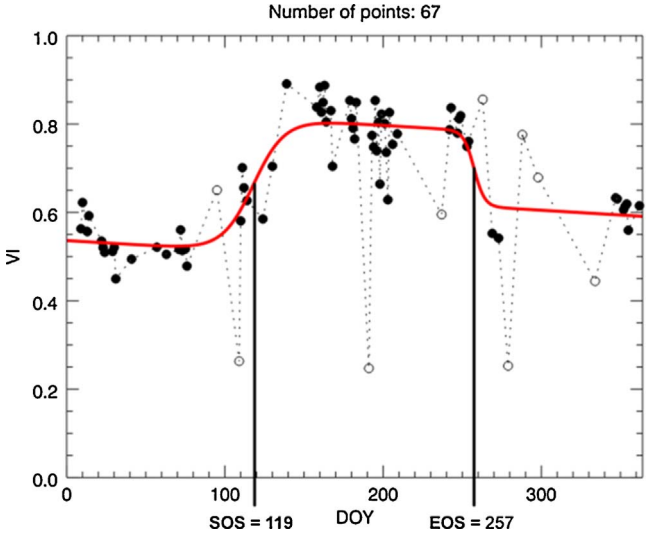

Fig. 4. NDVI for the plot CHP10, year 2006. Solid Circles: Daily NDVI values; Open circles: observations rejected by the median filter. Red line: fitted ndVI. Left vertical line: left inflection point (SOS), right vertical line: right inflection point (EOS). In this case, SOS and EOS dates were estimated to be on DOY 119 and 257, i.e. April, 25th and September 14th, respectively. (For interpretation of the references to colour in this figure legend, the reader is referred to the web version of this article.)

$$VI_t = p \cdot t + (a + c) + \frac{1}{2}(a - c) \cdot tanh[b \cdot (t - SOS)] - \frac{1}{2}(a - e) \cdot tanh[d \cdot (t - EOS)] \quad (5)$$

where VI_t is the fitted VI value at time t, SOS and EOS are the start of season and end of season date, and a, b, c, d, e, p, are the parameters of the curve. p accounts for the slight linear decrease in VI TS during winter and summer, observed in VI TS over deciduous broadleaf forests as underlined in previous studies (Soudani et al., 2012; Elmore et al., 2012; Hmimina et al., 2013; Melass et al., 2013).

The parameters of Eq. (5), including SOS and EOS, were estimated separately for each plot and for each year.

We tested all the possible solutions obtained by changing (with a time increment of 3 days) the initializations of the model's parameters

Table 2
Minimum and maximum values of the search windows.

	MIN [DOY]	MAX [DOY]	Range [days]
SOS	50 (19th Feb.)	185 (4th July)	135
EOS	210 (29th July)	355 (21st December)	135

SOS and EOS within a reasonable time period (search window), deduced from the average phenology of broadleaf forests in temperate regions of the Northern Hemisphere (Table 2). It resulted in a total of 2025 (45^2) combinations of SOS and EOS for each pixel/year.

For every combination of initialized SOS and EOS, a least square fitting was run. The minimum Root Mean Square Error (RMSE) between the given raw TS and each of the 2025 fitted TS, calculated for each of the 2025 solutions as in Eq. (6), was the driver to select the best fit.

$$RMSE_{FIT} = \sqrt{\frac{\sum_{n=1}^{n} (VI_{raw} - VI_{fit})^2}{n-1}} \quad (6)$$

SOS and EOS values corresponding to the selected solution were assigned to the site for the given year.

SOS or EOS estimation that fell out of the respective search windows were considered outlying estimations, and thus were excluded from the computation of the results. No considerations were made for climatically anomalous years.

3.4. Performance metrics

2001-2012 SOS and EOS estimations were generated with the procedure described above for each of the 6 VIs (EVI, NDVI, $WDRVI_{0.05}$, $WDRVI_{0.10}$, $WDRVI_{0.15}$, $WDRVI_{0.20}$), and for each of the considered TS (daily, $MOD13_{RAW}$, $MOD13_{AD}$, $MOD13_{ALIGNED}$, $MOD13_{DAILY}$), resulting in 30 SOS and EOS values for each pixel/year. Each pixel/year SOS/EOS estimation was compared with the four corresponding values (SOS and EOS for main tree species and understory) recorded within the RENECOFOR dataset (Table 1).

Results were summarized in terms of mean error (μ) and root mean square deviation (RMSD). μ is a measure of bias of satellite estimations respective to ground phenology, while RMSD is a measure of the real uncertainty of estimation. Metrics were aggregated and averaged on a per-year basis, i.e., for both SOS and EOS. All of the values (up to fifty) from every year were averaged, resulting in eight 12-year (i.e. 12 values) long TS. We assumed as best estimator (i.e. the best combination of VI and satellite data) the one that achieved the lowest μ and RMSD values, ideally $\mu = 0$ and RMSD ≤ 7.

In particular, for each comparison and ground parameters, μ was calculated as:

$$\mu = \frac{\sum_{y=1}^{12} \left(\frac{\sum_{i=1}^{50} (P_{ei,y} - P_{oi,y})}{50} \right)}{12} \quad (7)$$

where P_{ei} is the value of the phenological metric (SOS or EOS) estimated from satellite data, and P_{oi} is the same variable observed on the ground for plot i in year y. Negative bias ($\mu < 0$) means that MODIS-derived estimation was anticipated with respect to ground data. On the contrary, positive bias ($\mu > 0$) means that estimates were delayed. RMSD were calculated according to Eq. (8):

$$RMSD = \frac{\sum_{y=1}^{12} \left(\sqrt{\frac{\sum_{i=1}^{50} (P_{ei,y} - P_{oi,y})^2}{50-1}} \right)}{12} \quad (8)$$

Ground observations were carried out weekly and each observation was referred to the Monday of the week it belonged to. Consequently, if RMSD ≤ 7 days, it can be assumed that VI-based estimation was as precise as field surveys.

4. Results

4.1. Analysis of ground-based phenological observations

In order to allow a better understanding of the estimated SOS and EOS from MODIS time-series, descriptive statistics of ground-based phenological observations are shown (Fig. 5).

In general, SOS dates were less variable than EOS dates; moreover, SOS dates of main species were less dispersing than the understory's' SOS dates. Considering ground plots pooled all together for both SOS and EOS, it was clear that the average distance in time between variables was much less than their internal dispersion, making single phenological stages hard to separate from each other because of the overlaps (Fig. 5).

An overview of median time distances between ground phenological stages is shown in Table 3. Relative median temporal distances between ground parameters were calculated as relative difference respective to MSp 90% dates separately for both SOS and EOS.

Table 3 shows that, during spring, understory started generally earlier than main species trees. In fact, when understory reached the 90% level, main species just reached their 10% level.

The pattern shown by EOSs was much different: both understory's and main species' 10% events appeared on the same DOY on median, and a difference of only 1 day was found between main species and understory 90% yellowing stages.

4.2. Satellite estimates

Main results from all comparisons between estimated and observed SOS and EOS are summarized in Figs. 6–8. We considered "best SOS

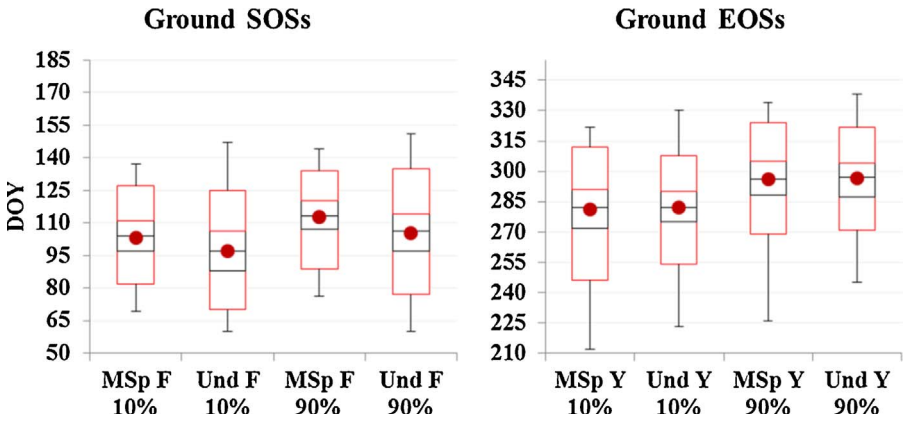

Fig. 5. Temporal distribution of the eight RENECOFOR phenological markers. Observations from all plots and all years were pooled. Left: Start of growing Season (SOSs); right: End of growing Season (EOSs). Black boxes: 1st to 3rd quartile, that is 50% of the values. Red boxes: 2.5th to 97.5th percentile, that embrace 95% of the observations. Black whiskers: minimum and maximum value of each distribution; red dots: average value. (For interpretation of the references to colour in this figure legend, the reader is referred to the web version of this article.)

Table 3
Timing of phenophases and distance in time relative to main species 90% flushing and yellowing. MSp 90% parameters were the reference. Highlighted in grey is the reference parameter.

SOSs			EOSs		
Phenophase	**Median [DOY]**	**Relative difference [days]**	**Phenophase**	**Median [DOY]**	**Relative difference [days]**
MSp F 10%	104	-9	**MSp Y 10%**	282	-14
Und F 10%	97	-16	**Und Y 10%**	282	-14
MSp F 90%	113	0	**MSp Y 90%**	296	0
Und F 90%	106	-7	**Und Y 90%**	297	1

combinations" those SOS VI/TS combinations that achieved simultaneously $\mu = 0 \pm 3$ days and RMSD ≤ 14 days. The first measure corresponds to unbiased estimations $\pm$ the length (in days) of 1 increment of procedure selecting the optimal fit; the latter corresponds to RMSD $\leq$ two times the accuracy of the RENECOFOR dataset. At the same time, since EOS estimations were poorer in quality than SOS, we doubled the ranges of acceptable μ and RMSD, considering "best EOS estimations" those that achieved simultaneously $\mu = 0 \pm 6$ days and RMSD ≤ 28 days. Results are illustrated in Fig. 6 for best SOS VI/TS combinations and in Figs. 7 and 8 for best EOS VI/TS

4.2.1. SOSs

Advanced greening of main species' canopies (MSp F 90%) was the only SOS ground parameter that the combination of VI and TS we considered could estimate meeting the above-mentioned quality requirements ($\mu = 0 \pm 3$ days and RMSD ≤ 14 days). Performances achieved by such combinations are reported in Fig. 6. VI/TS combinations are sorted according to a least-RMSD criterion (values are sorted first by increasing RMSD and then by increasing μ).

Among the best SOS results, all NDVI-based estimations were biased no more than 1 day in all comparisons with RMSDs ranging between 12–14 days. EVI, $WDRVI_{0.15}$ and $WDRVI_{0.20}$ showed 1–3 day biases, but lower RMSDs (10–12 days compared to 12–14).

Considering the RMSD-based rank we proposed in Fig. 6, EVI implemented from $MOD13_{DAILY}$ TS was the best-performing VI/TS combination, followed by $WDRVI_{0.20}$ implemented with $MOD13_{ALIGNED}$ TS. If a zero-bias approach is preferred, NDVI implemented with $MOD13_{RAW}$, $MOD13_{ALIGNED}$ and $MOD13_{DAILY}$ TS were the best-ranked solutions.

4.2.2. EOSs

Within the best EOS combinations reported in Figs. 7 and 8, considering only those referred to main trees phenology, we found that: a) $WDRVI_{0.05}$ lead to the best estimations of initial yellowing (MSp Y 10% parameter) across most TS; b) EVI lead to the best estimations of advanced yellowing (MSp Y 90%) across most comparisons.

Looking at the scatter plots, it is clear that the procedure did not allow precise EOS estimations because of the considerable errors at the single-estimation scale (sparse scatter plots).

Fig. 7 reports the best VI/TS combinations respective to early EOS comparisons. It shows that $WDRVI_{0.05}$ achieved the lower biases (1–2 days) and, when implemented based on $MOD13_{ALIGNED}$ TS, allowed the best performance (i.e. least RMSD AND least μ).

Fig. 8 shows the best VI/TS combinations regarding advanced EOS estimation (MSp Y 90%). According to the least-RMSD ranking, the best estimations were obtained by daily EVI, followed by EVI implemented on $MOD13_{AD}$ TS. NDVI performed slightly worse in terms of RMSD.

5. Discussions

The aim of this job was to test a new procedure to estimate SOS and EOS of temperate deciduous forest using MODIS data. We developed a new procedure that allowed us to significantly reduce arbitrarity when initializing the fitting parameters. In fact, this operation was made automatically assigning search windows based on the natural occurrence of SOS and EOS in forest. In this work, search windows were determined based on the dates contained in the RENECOFOR dataset. In our opinion, keeping stricter search windows would have led to better estimations. To further improve estimations quality, it would be useful to examine in deep the effect of gaps and noise in the original TS on the fitting algorithm, making it more robust and reliable. It would be interesting and useful for future works to examine the most critical pixel/years and evaluate: 1) if a given pixel/year is critical in all or most of the 12 years; and, 2) the causes of criticality (noise, gaps, anomalous shape of the raw TS).

From a technical point of view, in addition to the effects of temporal resolution and the distribution of the values in the VI time-series, the ability of the asymmetric double logistic function to describe finely the seasonal pattern of phenology in deciduous broadleaf forests is strongly dependent on the initialization of parameters. This is even more problematic since the model proposed in Hmimina et al. (2013) (Eq. (5)) adds a supplementary parameter to account for the monotonic decrease of VI over the winter and summer seasons. In this work, we developed an automatic per-pixel procedure that performed least square fittings of Eq. (5). In our procedure, a SOS and an EOS temporal search window were given, and day of year from such windows were used to sequentially initialize SOS and EOS values within the fitting procedure.

SOSs and EOSs were estimated for each combination of VI and TS (6 VIs by 5 TS = 30 combinations) and such SOS/EOS estimations were compared against the corresponding set of 4 SOS and 4 EOS parameters from the RENECOFOR dataset. Average bias (μ) and RMSD were the statistics we computed to evaluate the performance of every VI/TS combination.

In terms of errors (RMSD) between observed and predicted phenological metrics, SOS estimations were more precise and accurate than EOSs (10 days vs 22 days for best VI/TS combinations). This result agrees with the conclusion outlined in the MODIS phenology assessment works in the studies of Ganguly et al. (2014) and Zhang et al. (2006), that MODIS-based estimates of the end of growing season have larger uncertainty than the start of season. As noted in Soudani et al. (2012) and in Hmimina et al. (2013), the spring flush and leaf development and expansion in deciduous broadleaf forests are, in absence of extreme cold and freeze events, relatively fast and lasts between 20 and 40 days in beech and oak forests in France (Soudani et al., 2008; Soudani et al., 2012). This period is also surrounded by two periods, the unleafy season in winter and the maximum LAI stage in summer. During these two periods, VI temporal variations are relatively small, and consequently, the fit is more constrained and the inflection point is likely well determined.

From a vegetation point of view, the analysis of the pattern of ground data found that, on average, bud burst of understory was earlier in spring by about 7 days respective to main species. When main species

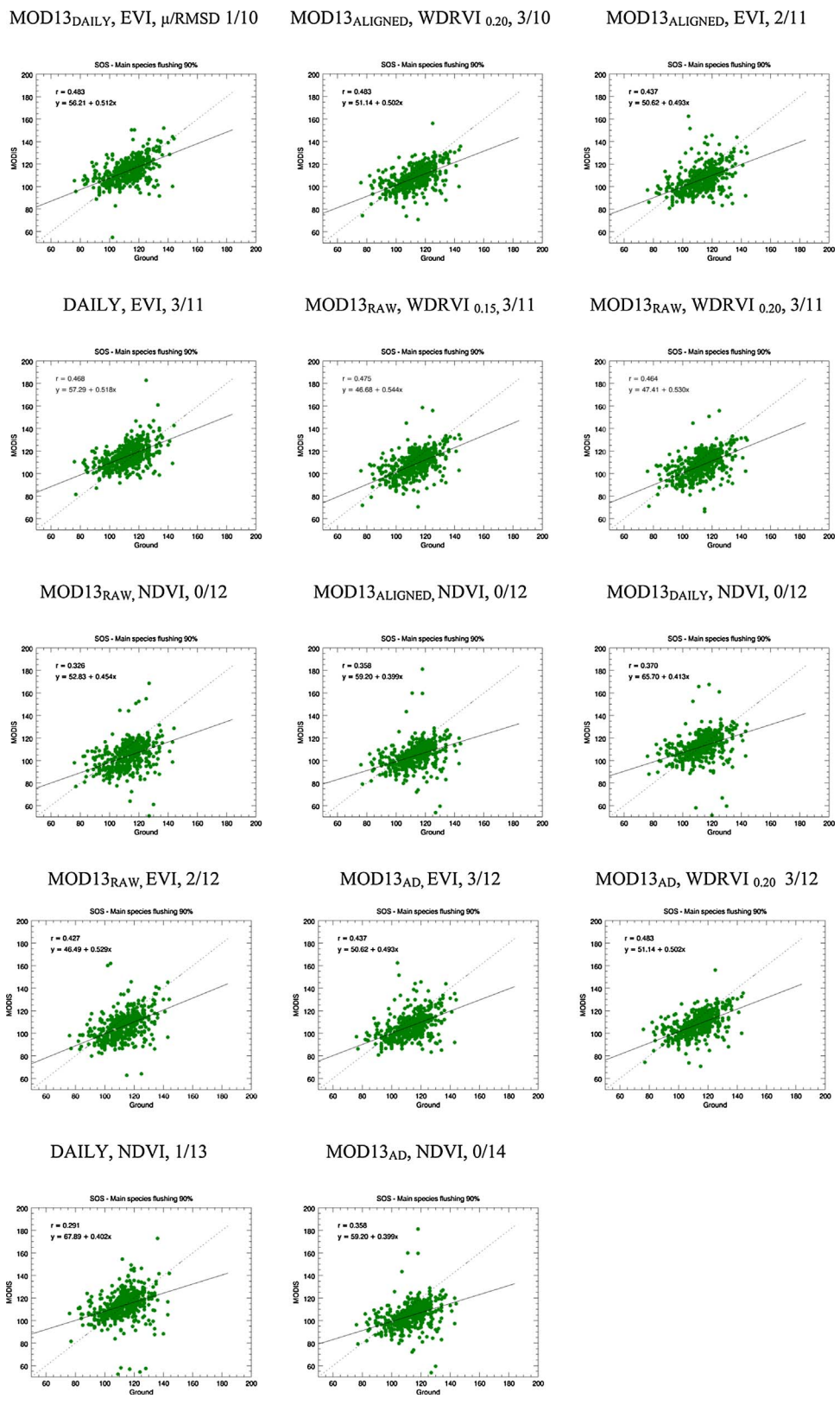

Fig. 6. SOS best results: MODIS/ground scatter plots of the best SOS estimations. The label above each plot contains, in the following order: TS type, VI, μ/RMSD (in days).

green up was beginning (10% F), understory was already reaching the 90% level. Since understory greening was generally earlier than that of overlaying canopies, the first increase of surface greenness observed from MODIS was potentially related to the understory rather than to overstory trees (our target). Despite this, the least biased SOS estimations were found respective to the advanced greening of main trees (MSp F 90%), meaning that MODIS estimations were more aligned to main trees greening rather than understory greening.

EOS estimations were affected by great uncertainty. This was possibly due to the greater complexity of autumnal leaf dynamics. Leaf yellowing, browning, marcescence and abscission, the mechanical influence of wind and precipitation, and the background effect of the soil

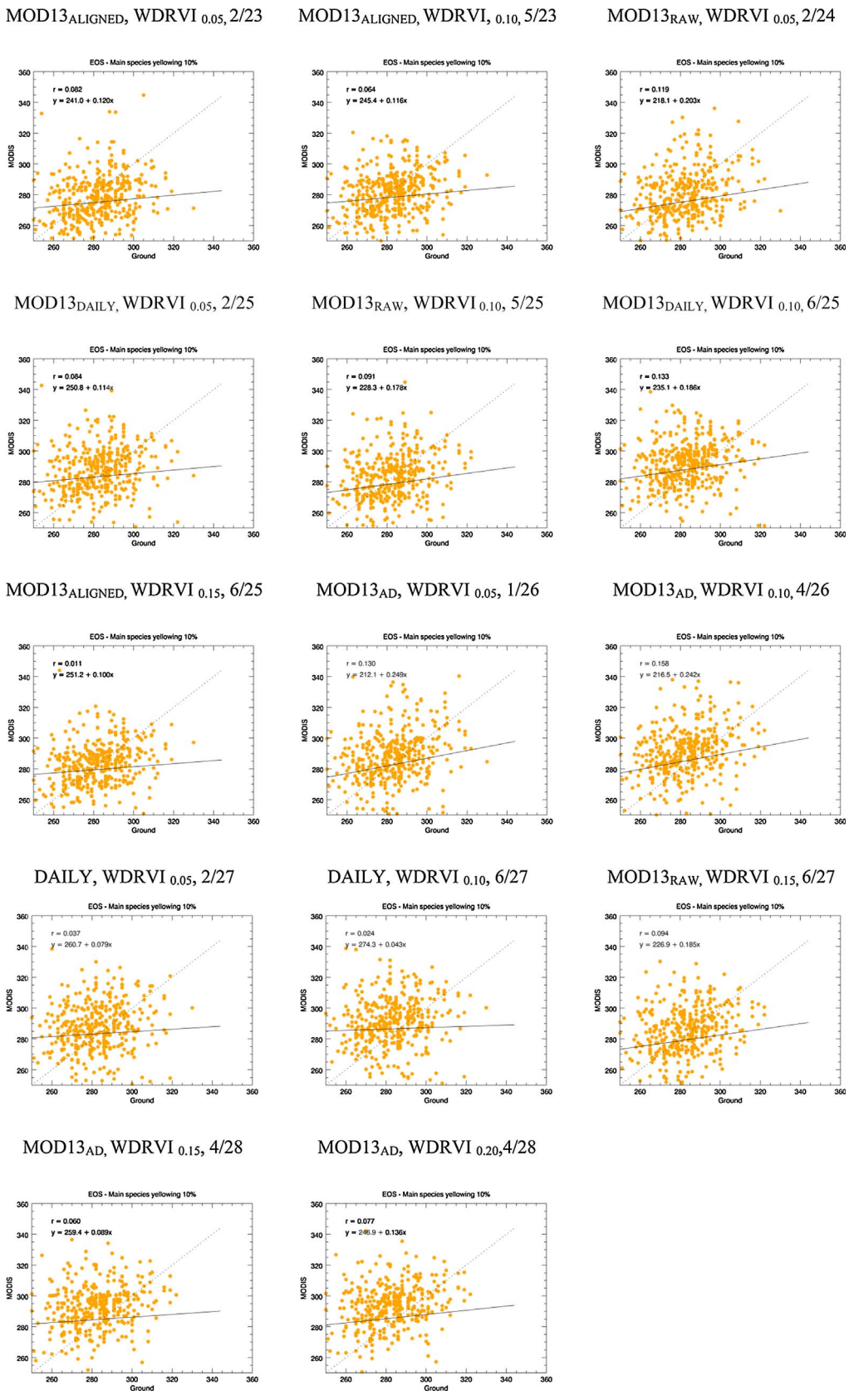

Fig. 7. Early EOS best results: MODIS/ground scatter plots of the best early EOS estimations. The label above each plot contains, in the following order: TS type, VI, μ/RMSD.

covered by freshly-fallen leaves make the decrease in values of VIs generally slower and less uniform in autumn than the increase in spring (Hmimina et al., 2013; Nagler et al., 2000; van Leeuwen and Huete, 1996).

In terms of bias, it can also be noted that, considering MSp F 90% vs MSp Y 90%, SOSs are both less and inversely biased than EOSs (1 day versus −5 days for best combinations). The small bias obtained SOSs means that the inflection point of the fit is a robust marker of the foliage

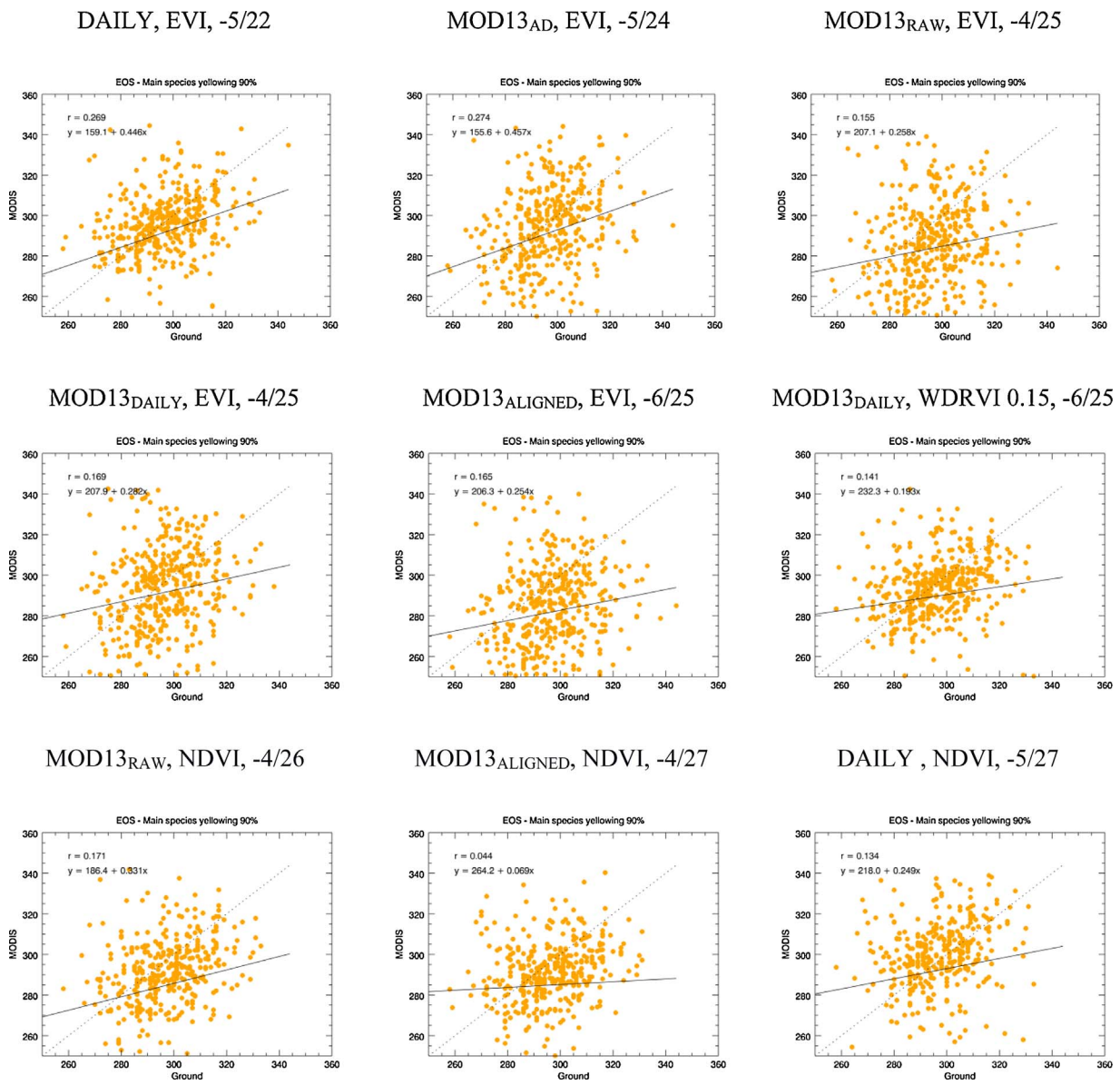

Fig. 8. Advanced EOS best results: MODIS/ground scatter plots of the best advanced EOS estimations. The label above each plot contains, in the following order: TS type, VI, μ/RMSD (in days).

development and expansion during the spring and confirms the results obtained in Hmimina et al. (2013) which focused on comparing MODIS and ground-based NDVI TS. The bias in SOSs obtained using the other VI/TS combinations are also positive indicating that MODIS-based estimates occur later than in situ phenological observations. By contrast, EOSs are negatively biased at MSp Y 90%, meaning that MODIS-based estimates anticipate the phase of onset of yellowing, but there are less and positively biased at MSp Y 10%. According to the RENECOFOR dataset, understory and main species yellowed almost together on average, and consistent differences were only recorded between initial and advanced yellowing. Satellite EOS estimations were less biased respective to early yellowing, meaning that the right inflection point of Eq. (5) was closer to the initial loss of greening rather than to advanced yellowing.

With regard to SOS, main trees advanced flushing (MSp F 90%) was the only phenological stage that could be estimated meeting the quality standard we set ($\mu = 0 \pm 3$ days, RMSD ≤ 14 days). Among the best SOS combinations (Fig. 6), NDVI allowed the least biased estimations (less than 1 day in every combination), but it showed slightly higher RMSDs compared to EVI and $WDRVI_{0.20}$. The best performance was obtained by EVI/$MOD13_{DAILY}$ TS, but the use of such a combination was very expensive in terms of computation time (365/366 values had to be fitted instead of less than 23 in the case of the other composite TS). Because of this, the use of both EVI or $WDRVI_{0.20}$ implemented from $MOD13_{ALIGNED}$ TS would be more suitable when computation time is a limiting factor.

In our study, the combination $WDRVI_{0.05}$/$MOD13_{ALIGNED}$ was the choice that allowed the best estimation of early yellowing (Fig. 7); daily EVI was instead the best estimator of advanced yellowing with performances very similar to those achieved by EVI/$MOD13_{AD}$ TS (Fig. 8). Advanced EOS estimations were generally less precise and accurate than early EOS estimations.

The phenomenon of senescence is a of great complexity and it is not surprising to note that compared to the spring leaf unfolding, there are less studies, both in vegetation phenology modeling and remote sensing, which were interested in the prediction of the date of senescence. Delpierre et al. (2009, 2015) emphasized the less attention given to the timing of leaf senescence, especially in modeling, and explained that this is probably due to the fact that the variability of the timing of leaf senescence seems to have less importance on the productivity of the

ecosystems since the senescence occurs when conditions of temperature and radiation are less favorable to photosynthesis. The authors also highlighted the complexity of the senescence phenomenon, which is slower, more diffuse and involves numerous processes. The same observation about the lack of studies interesting in remote sensing of leaf senescence can be made as pointed out in Elmore et al. (2012).

While satellite-based estimates of SOS appear to be sufficiently accurate and can be used with some confidence, estimates of EOS should be considered with great caution because of their large uncertainties. The use of such estimates in climate-vegetation interactions may lead to misinterpretation. Further remote sensing studies of the timing of senescence are therefore necessary. However, these studies must be based on phenological observations using ground-based sampling that considers that remote sensing-based phenology is a pixel-scale phenology. The sampling design must consider the spatial resolution of the sensors, the spatial distribution of overstory and understory species and between and within species phenological variations. The sampling design used in the RENECOFOR network, originally constituted to monitor the health of forests, allows gathering phenological observations at the stand scale.

EVI, NDVI, $WDRVI_{0.05}$ and $WDRVI_{0.20}$ showed similar performances across different TS in estimating a given phenological parameter (Fig. 6). In addition, daily MOD09 TS did not perform significantly better than MOD13 composite TS, if actual acquisition date is considered. In our opinion, this happened because the data (and, thus, the spectral content) underlying all TS was the same, i.e. daily reflectances. Combinations based on $MOD13_{RAW}$ TS should have led to estimations with greater errors because they did not account for acquisition dates. Despite this, they often appeared among the best results (Figs. 6–8). In our opinion, this was due to the temporal structure of the composite product. In a previous study (Testa et al., 2014), acquisition dates in chestnut woods in north-western Italy were found to be distributed around the middle of compositing periods, i.e. around their 8th and 9th day. In this work, we considered values from $MOD13_{RAW}$ TS (that did not account for acquisition dates) to be nominally placed on compositing periods' 8th days. This fact should not prevent any user from accounting for acquisition dates: if the global statistics presented in this work were similar among comparisons both accounting and not accounting for acquisition dates, errors could have been introduced at the single-plot scale and SOS and EOS estimations could have been affected (Testa et al., 2014). Because of this, we think the use of daily or composite date-corrected TS is more reliable (Hmimina et al., 2013).

6. Conclusions

The aim of this work was to find the best way to estimate SOS and EOS on deciduous, temperate forests. The fitting procedure we proposed here did not require the user to give an exact initialization of SOS and EOS parameters but only a reasonable time search window. In general, we would suggest the use of composite TS since they allowed us to achieve results somewhat better than daily TS, and were easier and faster to manage.

Despite VI/TS combinations based on raw MOD13Q1 VIs ($MOD13_{RAW}$ TS) often led to well ranked results, the use of date-corrected TS is highly recommended. We suggest the use of temporally aligned TS as described in Testa et al. (2014) since such a procedure, in this study, led to the best results in estimating both SOS and early EOS and was formally correct since it accounted for acquisition dates.

Referring to $MOD13_{ALIGNED}$ TS, the use of NDVI would allow unbiased SOS estimation with a 12 day precision; the use of $WDRVI_{0.20}$ increased SOS estimations' precision to 10 days, but estimates were postponed by 3 days on average. With regard to EOS, early yellowing was conveniently estimated by $WDRVI_{0.05}$ with a delay of 2 days and average error of 23 days

$WDRVI_{0.20}$ performed similarly to EVI in estimating the advanced greening of canopies and $WDRVI_{0.05}$ performed similarly to EVI in estimating canopies yellowing. Because of this, despite further investigations are needed, WDRVI could possibly be considered as an additional “continuity” index, together with NDVI, to the AVHRR dataset, since it does not require the blue band.

Acknowledgements

We are sincerely grateful to the editor and the reviewers for their thorough and helpful comments and suggestions that were usefully implemented to improve this work. Acknowledgments are due to the University of Idaho (Moscow, ID, United States) for the supplies made available in support of this work partial support was provided by USDA NIFA grant number 2011-32100-06016. MODIS imagery was obtained through the online Data Pool at the NASA Land Processes Distributed Active Archive Center (LP DAAC), USGS/Earth Resources Observation and Science (EROS) Center, Sioux Falls, South Dakota, USA (https://lpdaac.usgs.gov/data_access).

We acknowledge the *Réseau National de suivi à long terme des ECOsystèmes FORestiers* (RENECOFOR) for the ground data they gently and quickly supplied, allowing us to compare our results to ground measurements.

We thank Prof. Maria Carla Tabò and Dr. Axel Furlan for their valuable technical and mathematical support to this research.

References

Ahl, D.E., Gower, S.T., Burrows, S.N., Shabanov, N.V., Myneni, R.B., Knyazikhin, Y., 2006. Monitoring spring canopy phenology of a deciduous broadleaf forest using MODIS. Remote Sens. Environ. 104, 88–95.

Atkinson, P.M., Jeganathan, C., Dash, J., Atzberger, C., 2012. Inter-comparison of four models for smoothing satellite sensor time-series data to estimate vegetation phenology. Remote Sens. Environ. 123, 400–417.

Aubinet, M., Heinesch, B., Longdoz, B., 2002. Estimation of the carbon sequestration by a heterogeneous forest: night flux corrections: heterogeneity of the site and inter-annual variability. Global Change Biol. 8, 1053–1071.

Beaubien, E.G., Hall-Beyer, M., 2003. Plant phenology in western Canada: trends and links to the view fromspace. Environ. Monit. Assess. 88, 419–429.

Beck, P.S.A., Atzberger, C., Hogda, K.A., Johansen, B., Skidmore, A.K., 2006. Improved monitoring of vegetation dynamics at very high latitudes: a new method using MODIS NDVI. Remote Sens. Environ. 100, 321–334.

Bequet, R., Campioli, M., Kint, V., Vansteenkiste, D., Muys, B., Ceulemans, R., 2011. Leaf area index development in temperate oak and beech forests is driven by stand characteristics and weather conditions. Trees-Struct. Funct. 25, 935–946.

Brügger, R., Dobbertin, M., Krauchi, N., 2003. Phenological variation of forest trees. Phenol.: Integr. Environ. Sci. 39, 255–267.

Bradley, N.L., Leopold, A.C., Ross, J., Huffaker, W., 1999. Phenological changes reflect climate change in Wisconsin. Proc. Natl. Acad. Sci. U. S. A. 96, 9701–9704.

Bradley, B.A., Jacob, R.W., Hermance, J.F., Mustard, J.F., 2007. A curve fitting procedure to derive inter-annual phenologies from time series of noisy satellite NDVI data. Remote Sens. Environ. 106, 137–145.

Breda, N., Granier, A., Aussenac, G., 1995. Effects of thinning on soil and tree water relations, transpiration and growth in an oak forest (Quercus-petraea (Matt) Liebl). Tree Physiol. 15, 295–306.

Brooke, M.d.L., Jones, P.J., Vickery, J.A., Waldren, S., 1996. Seasonal patterns of leaf growth and loss, flowering and fruiting on a subtropical central Pacific island. Biotropica 28, 164–179.

Colombo, R., Busetto, L., Migliavacca, M., Cremonese, E., Meroni, M., Galvagno, M., Rossini, M., Siniscalco, C., di Cella, U.M., 2009. On the spatial and temporal variability of Larch phenological cycle in mountainous areas. Rivista Italiana Di Telerilevamento 41, 79–96.

Colombo, R., Busetto, L., Fava, F., Di Mauro, B., Migliavacca, M., Cremonese, E., Galvagno, M., Rossini, M., Meroni, M., Cogliati, S., Panigada, C., Siniscalco, C., di Cella, U.M., 2011. Phenological monitoring of grassland and larch in the Alps from Terra and Aqua MODIS images. Italian Journal of Remote Sensing-Rivista Italiana Di Telerilevamento 43, 83–96.

Cowie, J., 2007. Climate Change: Biological and Human Aspects. Cambridge University Press, Cambridge.

Crucifix, M., Betts, R.A., Cox, P.M., 2005. Vegetation and climate variability: a GCM modelling study. Clim. Dyn. 24, 457–467.

Davi, H., Soudani, K., Deckx, T., Dufrene, E., Le Dantec, V., Francois, C., 2006. Estimation of forest leaf area index from SPOT imagery using NDVI distribution over forest stands. Int. J. Remote Sens. 27, 885–902.

de Beurs, K.M., Henebry, G.M., 2004. Land surface phenology, climatic variation, and institutional change: analyzing agricultural land cover change in Kazakhstan. Remote Sens. Environ. 89 (4), 497–509. http://dx.doi.org/10.1016/j.rse.2003.11.006. 29 February 2004 ISSN 0034-4257.

de Beurs, K.M., Henebry, G.M., 2005. A statistical framework for the analysis of long image time series. Int. J. Remote Sens. 26, 1551–1573.

de Beurs, K.M., Henebry, G.M., 2010a. A land surface phenology assessment of the northern polar regions using MODIS reflectance time series. Can. J. Remote Sens. 36, S87–S110.
de Beurs, K.M., Henebry, G.M., 2010b. Spatio-temporal statistical methods for modelling land surface phenology. Phenol. Res.: Methods Environ. Clim. Change Anal. 177–208.
Defila, C., 1992. Phenology: an indicator for environmental changes. Schweizerische Rundschau fur Medizin Praxis = Revue suisse de medecine Praxis 81, 343–346.
Delpierre, N., Dufrêne, E., Soudani, K., Ulrich, E., Cecchini, S., Boé, J., François, C., 2009. Modelling interannual and spatial variability of leaf senescence for three deciduous tree species in France. Agric. For. Meteorol. 149, 938–948.
Delpierre, N., Vitasse, Y., Chuine, I., Guillemot, J., Bazot, S., Rutishauser, T., Rathgeber, C.K., 2015. Temperate and boreal forest tree phenology: from organ-scale processes to terrestrial ecosystem models. Ann. For. Sci. 1–21. http://dx.doi.org/10.1007/s13595-015-0477-6.
Demarée, G.R., Rutishauser, T., 2009. Origins of the word phenology. Eos Trans. Am. Geophys. Union 90, 1.
Eklundh, L., Johansson, T., Solberg, S., 2009. Mapping insect defoliation in Scots pine with MODIS time-series data. Remote Sens. Environ. 113, 1566–1573.
Elmore, A.J., Guinn, S.M., Minsley, B.J., Richardson, A.D., 2012. Landscape controls on the timing of spring, autumn: and growing season length in mid-Atlantic forests. Glob. Change Biol. 18, 656–674.
Elzinga, J.A., Atlan, A., Biere, A., Gigord, L., Weis, A.E., Bernasconi, G., 2007. Time after time: flowering phenology and biotic interactions. Trends Ecol. Evol. 22, 432–439.
European Environment Agency, 2004. Impacts of Europe's changing climate. An Indicator Based Assessment.
European Environment Agency, 2012. Climate change, impacts and vulnerability in Europe 2012. An Indicator-based Report.
Fabian, P., Menzel, A., 1998. Changes in phenology of trees in Europe. In: International Seminar on Causes and Consequences of Accelerating Tree Growth in Europe. Nancy, France. pp. 43–51.
Fenner, M., 1998. The phenology of growth and reproduction in plants. Perspect. Plant Ecol. Evol. Syst. 1, 78–91.
Fisher, J.I., Mustard, J.F., Vadeboncoeur, M.A., 2006. Green leaf phenology at Landsat resolution: scaling from the field to the satellite. Remote Sens. Environ. 100, 265–279.
Ganguly, S., Friedl, M.A., Tan, B., Zhang, X., Verma, V., 2014. Land surface phenology from MODIS: characterization of the collection 5 global land cover dynamics product. Remote Sens. Environ. 114, 1805–1816.
Gitelson, A.A., 2004. Wide dynamic range vegetation index for remote quantification of biophysical characteristics of vegetation. J. Plant Physiol. 161, 165–173.
Gond, V., de Pury, D.G.G., Veroustraete, F., Ceulemans, R., 1999. Seasonal variations in leaf area index, leaf chlorophyll, and water content; scaling-up to estimate fAPAR and carbon balance in a multilayer, multispecies temperate forest. Tree Physiol. 19, 673–679.
Granier, A., Ceschia, E., Damesin, C., Dufrene, E., Epron, D., Gross, P., Lebaube, S., Le Dantec, V., Le Goff, N., Lemoine, D., Lucot, E., Ottorini, J.M., Pontailler, J.Y., Saugier, B., 2000. The carbon balance of a young Beech forest. Funct. Ecol. 14, 312–325.
Gu, L.H., Post, W.M., Baldocchi, D., Black, T.A., Verma, S.B., Vesala, T., Wofsy, S.C., 2003. Phenology of vegetation photosynthesis. Phenol.: Integr. Environ. Sci. 39, 467–485.
Gutman, G., Ignatov, A., Olson, S., 1995. Global land monitoring using AVHRR time-series. Calibration Appl. Satell. Sens. Environ. Monit. 17, 51–54.
Henebry, G.M., 2013. Phenologies of North American grasslands and grasses. In: Schwartz, M.D. (Ed.), Phenology: An Integrative Environmental Science, 2e. Springer, pp. 197–210 Chapter 11.
Hird, J.N., McDermid, G.J., 2009. Noise reduction of NDVI time series: an empirical comparison of selected techniques. Remote Sens. Environ. 113, 248–258.
Hmimina, G., Dufrene, E., Pontailler, J.Y., Delpierre, N., Aubinet, M., Caquet, B., de Grandcourt, A., Burban, B., Flechard, C., Granier, A., Gross, P., Heinesch, B., Longdoz, B., Moureaux, C., Ourcival, J.M., Rambal, S., Saint Andre, L., Soudani, K., 2013. Evaluation of the potential of MODIS satellite data to predict vegetation phenology in different biomes: an investigation using ground-based NDVI measurements. Remote Sens. Environ. 132, 145–158.
Holben, B.N., 1986. Characteristics of maximum-value composite images from temporal AVHRR data. Int. J. Remote Sens. 7, 1417–1434.
Huete, A., Justice, C., van Leeuwen, W., 1999. MODIS Vegetation Index (MOD13) Algorithm Theoretical Basis Document.
Hufkens, K., Friedl, M., Sonnentag, O., Braswell, B.H., Milliman, T., Richardson, A.D., 2012. Linking near-surface and satellite remote sensing measurements of deciduous broadleaf forest phenology. Remote Sens. Environ. 117, 307–321.
Jönsson, P., Eklundh, L., 2002. Seasonality extraction by function fitting to time-series of satellite sensor data. Ieee Trans. Geosci. Remote Sens. 40, 1824–1832.
Jönsson, P., Eklundh, L., 2003. Seasonality Extraction from Satellite Sensor Data.
Jönsson, P., Eklundh, L., 2004. TIMESAT – a program for analyzing time-series of satellite sensor data. Comput. Geosci. 30, 833–845.
Jiang, Z., Huete, A.R., Didan, K., Miura, T., 2008. Development of a two-band enhanced vegetation index without a blue band. Remote Sens. Environ. 112, 3833–3845.
Keatley, M.R., Fletcher, T.D., 2003. In: Schwartz, K.A.p. M.D. (Ed.), Australia in Phenology: An Integrative Environmental Science, pp. 27–44.
Koch, E., Bruns, E., Chmielewski, F.-M., Defila, C., Lipa, W., Menzel, A., 2008. Guidelines for plant phenological observations. WMO Technical Commission for Climatology, Open Program Area Group on Monitoring and Analysis of Climate Variability and Change (OPAG2).
LP DAAC, 2014. Surface Reflectance Daily L2G Global 1 km and 500 m – MOD09GA User Guide. http://modis-sr.ltdri.org/guide/MOD09_UserGuide_v1_3.pdf.
Liang, L., Schwartz, M.D., 2009. Landscape phenology: an integrative approach to seasonal vegetation dynamics. Landsc. Ecol. 24, 465–472.
Liang, L., Schwartz, M.D., Fei, S., 2011. Validating satellite phenology through intensive ground observation and landscape scaling in a mixed seasonal forest. Remote Sens. Environ. 115, 143–157.
Lieberman, D., Milton, L., 1984. The causes and consequences of synchronous flushing in a dry tropical forest. Biotropica 16, 193–201.
Lieth, H., 1974. Phenology and Seasonality Modeling. Springer-Verlag, New York, N.Y., U.S.A.; Heidleberg, West Germany.
Melass, E.K., Friedl, M.A., Zhu, Z., 2013. Detecting interannual variation in deciduous broadleaf forest phenology using Landsat TM/ETM+ data. Remote Sens. Environ. 132, 176–185.
Menzel, A., Fabian, P., 1999. Growing season extended in Europe. Nature 397 659-659.
Morisette, J.T., Richardson, A.D., Knapp, A.K., Fisher, J.I., Graham, E.A., Abatzoglou, J., Wilson, B.E., Breshears, D.D., Henebry, G.M., Hanes, J.M., Liang, L., 2009. Tracking the rhythm of the seasons in the face of global change: phenological research in the 21st century. Front. Ecol. Environ. 7, 253–260.
Morren, C., 1849. Le Globe, le Temps et la Vie.
Nagler, P.L., Daughtry, C.S.T., Goward, S.N., 2000. Plant litter and soil reflectance. Remote Sens. Environ. 71, 207–215.
Noormets, A., 2009. Phenology of ecosystem processes: applications in global change research. Phenology of Ecosystem Processes: Applications in Global Change Research.
Nordli, O., Wielgolaski, F.E., Bakken, A.K., Hjeltnes, S.H., Mage, F., Sivle, A., Skre, O., 2008. Regional trends for bud burst and flowering of woody plants in Norway as related to climate change. Int. J. Biometeorol. 52, 625–639.
Parmesan, C., Galbraith, H., 2004. Observed Impacts of Global Climate Change in the US. Pew Center on Global Climate Change, Arlingtonk, VA p. 56.
Penuelas, J., Filella, I., 2001. Phenology – responses to a warming world. Science 294, 793-.
Penuelas, J., Rutishauser, T., Filella, I., 2009. Phenology feedbacks on climate change. Science 324, 887–888.
Ratkowsky, D.A., 1983. Nonlinear Regression Modeling—A Unified Practical Approach.
Richardson, A.D., Bailey, A.S., Denny, E.G., Martin, C.W., O'Keefe, J., 2006. Phenology of a northern hardwood forest canopy. Glob. Change Biol. 12, 1174–1188.
Richardson, A.D., Keenan, T.F., Migliavacca, M., Ryu, Y., Sonnentag, O., Toomey, M., 2013. Climate change, phenology: and phenological control of vegetation feedbacks to the climate system. Agric. For. Meteorol. 169, 156–173.
Rodriguez-Galiano, V.F., Dash, J., Atkinson, P.M., 2015. Intercomparison of satellite sensor land surface phenology and ground phenology in Europe. Geophys. Res. Lett. 42, 2253–2260.
Rosenzweig, C., Casassa, G., Karoly, D.J., Imeson, A., Liu, C., Menzel, A., Rawlins, S., Root, T.L., Seguin, B., Tryjanowski, P., 2007. Assessment of observed changes and responses in natural and managed systems. Climate Change 2007: Impacts, Adaptation and Vulnerability. Contribution of Working Group II to the Fourth Assessment Report of the Intergovernmental Panel on Climate Change. Cambridge UP, Cambridge, UK, pp. 79–131.
Ruml, M., Vulić, T., 2005. Importance of phenological observations and predictions in agriculture. J. Agric. Sci. 50 (2), 217–225.
Sarvas, R., 1972. Investigations on the Annual Cycle of Development of Forest Trees I. Autumn Dormancy and Winter Dormancy. Communicationes Instituti Forestalis Fenniae, pp. 76.
Sarvas, R., 1974. Investigations on the Annual Cycle of Development of Forest Trees II. Active Period. Communicationes Instituti Forestalis Fenniae, pp. 84.
Schaber, J., Badeck, F.-W., 2005. Plant phenology in Germany over the 20th century. Reg. Environ. Change 5, 37–46.
Schwartz, M.D., 1998. Green-wave phenology. Nature 394, 839–840.
Sesnie, S.E., Dickson, B.G., Rosenstock, S.S., Rundall, J.M., 2012. A comparison of Landsat TM and MODIS vegetation indices for estimating forage phenology in desert bighorn sheep (Ovis canadensis nelsoni) habitat in the Sonoran Desert, USA. Int. J. Remote Sens. 33, 276–286.
Setiawan, Y., Yoshino, K., Prasetyo, L.B., 2014. Characterizing the dynamics change of vegetation cover on tropical forestlands using 250 m multi-temporal MODIS EVI. Int. J. Appl. Earth Obs. Geoinf. 26, 132–144.
Solano, R., Didan, K., Jacobson, A., Huete, A., 2010. MODIS Vegetation Index User's Guide (MOD13 Series). Version 2.00, (Collection 5). Vegetation Index and Phenology Lab – The University of Arizona. http://vip.arizona.edu/documents/MODIS/MODIS_VI_UsersGuide_01_2012.pdf.
Song, Y., Njoroge, J.B., Morimoto, Y., 2013. Drought impact assessment from monitoring the seasonality of vegetation condition using long-term time-series satellite images: a case study of Mt. Kenya region. Environ. Monit. Assess. 185, 4117–4124.
Soudani, K., Francois, C., le Maire, G., Le Dantec, V., Dufrene, E., 2006. Comparative analysis of IKONOS, SPOT: and ETM+ data for leaf area index estimation in temperate coniferous and deciduous forest stands. Remote Sens. Environ. 102, 161–175.
Soudani, K., le Maire, G., Dufrene, E., Francois, C., Delpierre, N., Ulrich, E., Cecchini, S., 2008. Evaluation of the onset of green-up in temperate deciduous broadleaf forests derived from moderate resolution imaging spectroradiometer (MODIS) data. Remote Sens. Environ. 112, 2643–2655.
Soudani, K., Hmimina, G., Delpierre, N., Pontailler, J.Y., Aubinet, M., Bonal, D., Caquet, B., de Grandcourt, A., Burban, B., Flechard, C., Guyon, D., Granier, A., Gross, P., Heinesh, B., Longdoz, B., Loustau, D., Moureaux, C., Ourcival, J.M., Rambal, S., Saint Andre, L., Dufrene, E., 2012. Ground-based Network of NDVI measurements for tracking temporal dynamics of canopy structure and vegetation phenology in different biomes. Remote Sens. Environ. 123, 234–245.
Studer, S., Stockli, R., Appenzeller, C., Vidale, P.L., 2007. A comparative study of satellite and ground-based phenology. Int. J. Biometeorol. 51, 405–414.
Testa, S., Mondino, E.C.B., Pedroli, C., 2014. Correcting MODIS 16-day composite NDVI time-series with actual acquisition dates. Eur. J. Remote Sens. 47, 285–305.
Thayn, J.B., Price, K.P., 2008. Julian dates and introduced temporal error in remote

sensing vegetation phenology studies. Int. J. Remote Sens. 29, 6045–6049.
Thomas, K.A., Denny, E.G., Miller-Rushing, A.J., Crimmins, T.M., Weltzin, J.F., 2010. The national phenology monitoring system v0.1. USA-NPN Technical Series 2010-001.
Tucker, Compton J., 1979. Red and photographic infrared linear combinations for monitoring vegetation. Remote Sens. Environ. 8 (2), 127–150 Elsevier.
van Leeuwen, W.J.D., Huete, A.R., 1996. Effects of standing litter on the biophysical interpretation of plant canopies with spectral indices. Remote Sens. Environ. 55, 123–138.
Viña, A., Gitelson, A.A., 2005. New developments in the remote estimation of the fraction of absorbed photosynthetically active radiation in crops. Geophys. Res. Lett. 32, 4.
Villegas, D., Aparicio, N., Blanco, R., Royo, C., 2001. Biomass accumulation and main stem elongation of durum wheat grown under Mediterranean conditions. Ann. Bot. 88, 617–627.
Vitasse, Y., Basler, D., 2013. What role for photoperiod in the bud burst phenology of European beech. Eur. J. For. Res. 132, 1–8.
Wolfe, R.E., Roy, D.P., Vermote, E., 1998. MODIS land data storage, gridding: and compositing methodology: level 2 grid. Ieee Trans. Geosci. Remote Sens. 36, 1324–1338.
World Meteorological Organization, 2006. Systematic observation requirements for satellite-based products for climate. In: programme, U.n.e., science, I.c.f. (Eds.), Supplemental Details to the Satellite-Based Component of the Implementation Plan for the Global Observing System for Climate in Support of the UNFCCC.
Xiao, X.M., Braswell, B., Zhang, Q.Y., Boles, S., Frolking, S., Moore, B., 2003. Sensitivity of vegetation indices to atmospheric aerosols: continental-scale observations in Northern Asia. Remote Sens. Environ. 84, 385–392.
Zhang, X.Y., Friedl, M.A., Schaaf, C.B., Strahler, A.H., Hodges, J.C.F., Gao, F., Reed, B.C., Huete, A., 2003. Monitoring vegetation phenology using MODIS. Remote Sens. Environ. 84, 471–475.
Zhang, X., Friedl, M.A., Schaaf, C.B., 2006. Global vegetation phenology from Moderate Resolution Imaging Spectroradiometer (MODIS): Evaluation of global patterns and comparison with in situ measurements. J. Geophys. Res. 111, G04017. http://dx.doi.org/10.1029/2006JG000217.
Zhang, X., Friedl, M.A., Schaaf, C.B., 2009. Sensitivity of vegetation phenology detection to the temporal resolution of satellite data. Int. J. Remote Sens. 30, 2061–2074.